Comparative study on the chemical stability of Fe_3O_4 and $NiFe_2O_4$ in molten salts

P. Meyer[a], M. Gibilaro[a,*], L. Massot[a], I. Pasquet[b], P. Tailhades[b], S. Bouvet[c], P. Chamelot[a]

[a] Université de Toulouse-UPS, Laboratoire de Génie Chimique UMR CNRS 5503, 118 Route de Narbonne, 31062 Toulouse Cedex 09, France
[b] Institut Carnot Chimie Balard Cirimat, UMR CNRS 5085, Université de Toulouse – UPS, 118 Route de Narbonne, 31062 Toulouse Cedex 09, France
[c] Rio Tinto Aluminium Pechiney Aluval, 725 Rue Aristide Berges, BP-7, 38341 Voreppe, France

Keywords:
Ceramics
Electrode materials
Molten salts
Spinel
Kinetics
Scanning electron microscopy

A B S T R A C T

Tests on $Ni_xFe_{3-x}O_4$ spinels, considered as promising materials in the aluminium production, were performed on Fe_3O_4 and $NiFe_2O_4$. First, $FeAl_2O_4$ aluminate was spontaneously formed by Fe_3O_4 immersion at 960 °C, due to Fe^{3+}/Al^{3+} substitution into the spinel structure. Then, stability of aluminate compound was investigated into cryolite melt and results showed a rapid dissolution when the aluminate composition tends to $FeAl_2O_4$. Kinetic studies demonstrated that the spinel dissolution was around twentyfold higher than aluminate formation, confirming the micrographic observation. To prevent it, nickel was added in the spinel structure up to $NiFe_2O_4$ and no dissolution was observed.

1. Introduction

Hall-Héroult process produces aluminium by alumina electrolysis (Al_2O_3) in a molten mixture of cryolite ($Na_3AlF_6 – AlF_3 – CaF_2 – Al_2O_3$) at high temperature (960 °C) [1]:

$$2Al_2O_{3(l)} + 3C_{(s)} \rightarrow 4Al_{(l)} + 3CO_{2(g)} \quad (1)$$

Aluminium metal is obtained at the cathode and oxygen ions react with a reactive carbon anode to produce carbon dioxide. One of the key challenges for the aluminium industry is to replace CO_2 by O_2 release on an inert anode.

The basic requirements for an inert anode are listed below [2]:

High thermo-mechanical properties (shock and thermal gradient resistances)
High electrical conductivity ($> 80\ S{\cdot}cm^{-1}$)
High stability to oxidation and fluoration at high temperature
Consumption rate lower than 1 cm/year for $0.8\ A/cm^2$

Since many years, three types of inert anode for aluminium electrolysis have been examined: metals or alloys [3–5], oxides [6,7], or cermets (materials with both oxide and metallic phases) [8,9].

No satisfying material has been found yet to be used as oxygen-evolving anodes.

Oxides were envisaged due to their excellent chemical stability and high melting point. However, few oxides are conductive enough to be used as an electrical conductor. Tin dioxide [10] was studied in cryolite and electrolysis tests evidenced a very limited mechanical resistance, leading to crack propagations, and an important pollution of the aluminium metal (Sn > 1400 ppm) [10].

Mixed spinel oxides $Ni_xFe_{3-x}O_4$ ($0 < x < 1$) have been investigated since the 90's for their good mechanical resistance and conductivity [11]. Spinel structure is characterized by an electron hopping conduction mode [12], occurring in the same sub-lattice between two adjacent metallic cations of the same element with oxidation states differing by one unit (eg: Fe^{2+}/Fe^{3+}).

De Young et al. [13] demonstrated at 1000 °C that both spinels conductivity and stability depend on the nickel amount and that these important characteristics vary in the opposite direction: conductivity decreases and stability increases from Fe_3O_4 (x = 0) to $NiFe_2O_4$ (x = 1).

Xiao et al. [14] worked on the degradation rate of nickel ferrite in cryolite-based melt at 980 °C under anodic polarization. The authors examined the influence of the composition and porosity of the material, the Al_2O_3 content and the cryolitic ratio, and concluded that $NiFe_2O_4$ spinels were only slightly deteriorated during the electrochemical process.

Cassayre et al. [15] also studied $Ni_xFe_{3-x}O_4$ (x = 0.22, 0.48, 0.72, 0.78, and 0.9) and Fe_2O_3 formation was revealed at the grain boundaries. Moreover, Ni rich compositions exhibited a better resistance to degradation, confirming the work of De Young et al. [13]. Verwey et al. [12] completed the investigation by highlighting a preferential dissolution of Fe into the $NiFe_2O_4$ phase, leading to a non-uniform

* Corresponding author.
E-mail address: gibilaro@chimie.ups-tlse.fr (M. Gibilaro).

Table 1
State of the art on nickel ferrite anodes.

	Spinel composition	Electrolyte			Atmosphere	Temperature (°C)
		CR	wt% CaF_2	wt% Al_2O_3		
Olsen [11]	$NiFe_2O_4$	2.2	10	8	Air	960
De Young [13]	$NiFe_2O_4$	0.7–2.8	0	0.5– 6.5	Air	965–1025
Xiao [14]	$NiFe_2O_4$	1.38; 1.43	0; 5	5; 10; 15	Argon; CO_2; air	980
Cassayre [15]	$Ni_xFe_{3-x}O_4$ (x = 0.22; 0.48; 0.72; 0.78; 0.90)	2.2	5	9	Argon	960
Jentoftsen [16]	$FeAl_2O_4$ $NiAl_2O_4$ $NiFe_2O_4$	3	0	10	Argon	1020
Baogang [17]	$NiFe_2O_4$	2.3	5	7.43	Air	960
Nightingale [18]	$NiFe_2O_4$	2.68; 2.75	5; 6	6; 10	Argon	980

degradation of $NiFe_2O_4$ grains, and suggesting a $Ni_xFe_{3-x-y}Al_yO_4$ aluminate type formation at the anode surface.

An aluminate formation was also proposed by Jentoftsen et al. [16] between iron oxide and alumina:

$$FeO_{(s)} + Al_2O_{3(cry)} = FeAl_2O_{4(s)} \quad (2)$$

Gibbs energy of $FeAl_2O_4$ formation at 1020 °C ($\Delta G_f = -17.6\ kJ{\cdot}mol^{-1}$) shows a spontaneous formation of aluminate when contacting the cryolite salt and the material without polarization. Moreover, the authors suggested that this aluminate phase is soluble into the molten cryolite. To resume, the different anode materials and experimental conditions are gathered in Table 1.

A lot of works on nickel iron spinels degradation under polarization have been carried out and some studies without polarization showed that iron oxides are not chemically stable into molten cryolite. No global degradation mechanism was proposed in the bibliography as the anode consumption is a complex phenomenon, resulting from electrochemical reactions (phases oxidation during polarization) and chemical reactions (spontaneous aluminate formation). This publication is mainly focused on the aluminate formation mechanism and its stability, starting from spinel oxides without polarization.

The aim of this work is to determine the influence of Ni content in $Ni_xFe_{3-x}O_4$ spinels chemical stability in molten fluorides (x = 0 and x = 1). Fe_3O_4 and $NiFe_2O_4$ pellets were manufactured in house by sintering under air and argon after shaping by uniaxial pressing. Immersion tests with different durations were performed into molten salts at 960 °C. Spinels were analyzed after immersion by optical microscopy (dimension measurements) and SEM (Scanning Electron Microscopy) coupled with EDX (Energy Dispersive X-ray Spectroscopy) to determine the composition of the different phases. Kinetics studies of aluminate formation and material dissolution were performed on Fe_3O_4 and $NiFe_2O_4$ spinels and a reaction mechanism of the oxide behaviour without polarization is proposed.

2. Materials and methods

2.1. Analytical techniques

Sintered pellets were analyzed by X-ray diffraction. Measurements at room temperature were recorded on a Bruker D4-ENDEAVOR diffractometer, in the Bragg–Brentano geometry, using the Cu Kα radiations ($K\alpha_1 = 0.15405$ nm and $K\alpha_2 = 0.15443$ nm) (40 kV, 40 mA). Diffraction intensities were measured by scanning from 10° to 100° (2θ) with a step size of 0.02° (2θ). The oxides were embedded in cold conductive resin and polished for surface analysis of their cross-sections. This analysis is repeated three times by sample, with a very good reproducibility. Scanning electron microscope (SEM) with a Backscattered Electron (BSE) detector observations coupled with EDX analysis were performed on a PhenomWorldXL and EDX analysis parameters are gathered in Table 2. For dimensional measurements, an optical metallographic microscope ZEISS AXIO Imager.M2m was used.

Table 2
EDX analysis parameters.

Electron beam voltage	15 kV
Work Distance	9.7 mm
Emission current	77 µA

2.2. Chemicals and bath preparations

The cryolite melt is composed of Na_3AlF_6 (Carlo Erba, purity 99.99%), with an addition of 11 wt% excess of AlF_3 (ProChem Inc, purity 99.99%) and 5 wt% of CaF_2 (Apollo Scientific, purity 99.99%), leading to a cryolitic ratio (CR) of 2.2. Alumina saturation was achieved by addition of 8 wt% of alumina (Alfa Aesar, purity 99%). The salt mixture was heated until 960 °C under argon atmosphere.

The LiF – CaF_2 eutectic melt is composed of 56 wt% LiF (Apollo Scientific, purity 99.99%), with 44 wt% of CaF_2 (Apollo Scientific, purity 99.99%). AlF_3 (ProChem Inc, purity 99.99%) was added as a solute, at 2.5 wt% and 5 wt%. The salt cleaning procedure is the following: the mixture was heated under vacuum (1 mbar) up to 700 °C and then kept constant at 960 °C.

2.3. Experimental set up

The salts are contained in a vitreous carbon crucible, placed in a graphite liner protecting the inside wall of a cylindrical vessel made of refractory steel. The cell is closed by a stainless steel lid cooled by circulating water. A schematic diagram of the experimental setup has already been presented in previous article [19]. The gaseous atmosphere is inert argon (4.5 grade).

2.4. Spinel samples preparation

Pure dense ceramics of Fe_3O_4 and $NiFe_2O_4$ were prepared from hematite α-Fe_2O_3 (Alfa Aesar, purity 99.5%) and nickel ferrite (Orrion Chemicals Metalchem, 99.9%) powders respectively. The first step is to grow up the grain to make the shaping and the sintering easier. Fe_2O_3 and $NiFe_2O_4$ powders were annealed at 800 °C for 1 h under air atmosphere.

Polyvinylic alcohol (PVA) was added to oxide powders up to 4% of PVA dry extract. PVA and oxide powders were shaped by uniaxial pressing under 200 MPa to prepare 20 mm diameter pellets. The ratio of the oxide surface area (1.3 cm^2) to the bath volume (95.7 cm^3) is close to 0.01 $cm^2{\cdot}cm^{-3}$ and then small enough order to prevent bath chemical variations and to be lower than the solubility limit. The organic binder was removed by heat treatment at 600 °C for 5 h under air flow. The pellets were then sintered at different high temperatures depending

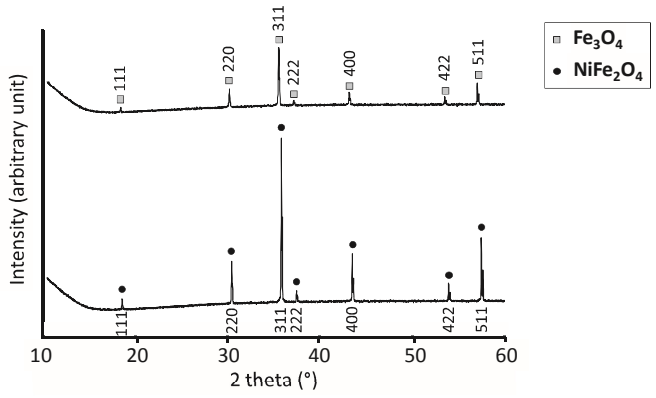

Fig. 1. XRD patterns of Fe_3O_4 and $NiFe_2O_4$ samples. Bragg peak indices are indicated for both structures: cubic with the Fd-3m space group.

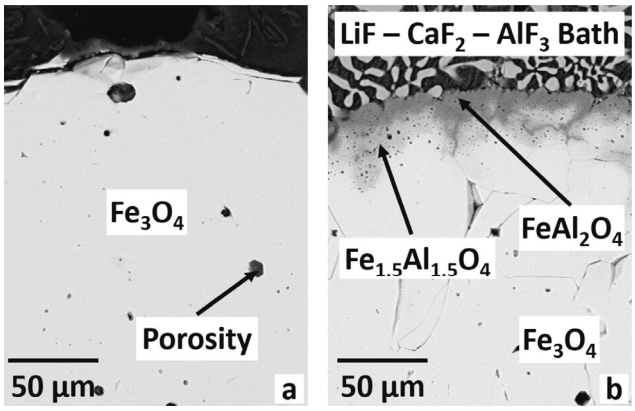

Fig. 2. SEM images of Fe_3O_4 pellet before (a) and after immersion (b) into LiF – CaF_2 – AlF_3 bath at 960 °C for 14 h.

on the atmosphere:

- Fe_2O_3 was reduced at 1150 °C for 2 h (100 °C/h) and then sintered at 1350 °C for 10 h in argon atmosphere. The cooling rate was 120 °C/h.
- $NiFe_2O_4$ ceramics were sintered at 1350 °C for 5 h in air atmosphere according to the thermal treatment reported by Corso et al. [20]. To reduce a part of Fe^{3+} into Fe^{2+} and to prevent a monoxide phase formation, $NiFe_2O_4$ pellets were then annealed at 1150 °C for 10 h in argon atmosphere.

The obtained closed porosity is around 5%.

Fig. 1 displays X-ray diffraction patterns obtained for these pellets after heat treatment. The patterns show diffraction peaks corresponding to cubic spinel structure of Fe_3O_4 (JCPDS 01-075-1372) and $NiFe_2O_4$ (JCPDS 00-054-0964) without any secondary phase.

Oxide lattice parameters were determined with d-spacings obtained from XRD patterns:

- Fe_3O_4: a = 8.40910 Å, in agreement with the literature data a = 8.39580 Å [21].
- $NiFe_2O_4$: a = 8.33467 Å, in agreement with the literature data (a = 8.33673 Å [22].

In this spectrum, peaks are doubled due to the K alpha Cu radiation. As the sample is not a powder but a pellet, an asymmetry for high 2 theta angles is observed and is due to non-parallel diffraction plans.

3. Results and discussions

3.1. $FeAl_2O_4$ aluminate formation from Fe_3O_4

As demonstrated by Jentoftsen et al. [16], $FeAl_2O_4$ aluminate is spontaneously formed at the material/salt interface by reaction between iron oxide and alumina [Eq. (2)], and this aluminate is supposed to be soluble in cryolite. A first immersion test was realised on Fe_3O_4 in cryolite. This experiment showed an aluminate formation and a decrease of the sample volume, confirming Jentoftsen hypothesis (Fe_3O_4 reaction and dissolution). However, the composition of this soluble aluminate couldn't be determined and the experiment was repeated many times: it has been decided to change the solvent composition. LiF – CaF_2 – AlF_3 was selected for its similar properties [23] at the operating temperature. To prove the $FeAl_2O_4$ formation, Fe_3O_4 pellet was immersed into LiF – CaF_2 – AlF_3 (2.5 wt%) bath at 960 °C for 14 h and micrographic analyses of the pellet before and after immersion are presented in Fig. 2.

A dense and homogeneous layer (15 µm) of $FeAl_2O_4$ is observed at the material/bath interface. A line scan of the $Fe_{3-x}Al_xO_4$ layer is

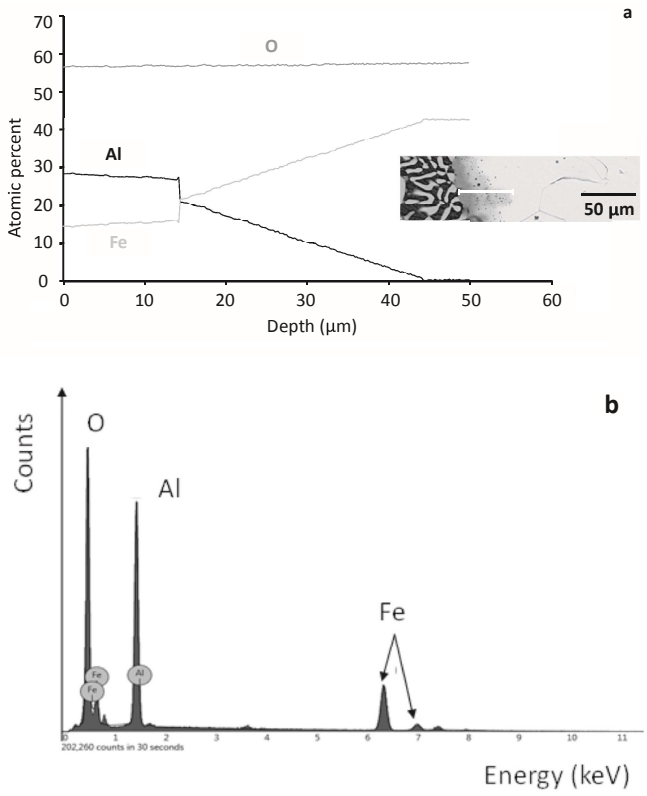

Fig. 3. Line scan of $Fe_{3-x}Al_xO_4$ layer (a) and EDX spectrum of one analyzed spinel (b).

Table 3
Data extracted from EDX analysis of one spinel sample.

Element Number	Element Symbol	Element Name	Atomic Concentration	Error
8	O	Oxygen	57.1	0.1
13	Al	Aluminium	28.6	0.0
26	Fe	Iron	14.3	0.0

provided in Fig. 3a. where a continuous insertion of aluminium is observed. The spinel composition is calculated from EDX results in Fig. 3b where the atomic percent of each element is obtained in Table 3: Fe, Al, O.

The unconsidered peaks correspond to the C element, which is the main compound of our mounting resin.

The analysis gives the following phase composition:

$Fe_{0.14}Al_{0.29}O_{0.57}$

As a spinel is composed of 4 oxygen atoms and 3 metallic cations, M_3O_4, a direct correspondence between the atomic percent of O determined from EDX and the number of O defined in a spinel can be found:

$$O = 57.1\%_{at} \rightarrow x_O = 4$$

$$Al = 28.6\%_{at} \rightarrow x_{Al} = 4*28.6/57.1 = 2$$

$$Fe = 14.3\%_{at} \rightarrow x_{Fe} = 4*14.3/57.1 = 1$$

The spinel composition is then $FeAl_2O_4$. The same procedure was used for all the spinel composition determination.

Below this layer, a second one made of $Fe_{1.5}Al_{1.5}O_4$ can be observed. The formation of these aluminates at high temperature can be explained by considering the spinel crystallographic structure. In this face centered cubic structure, the existence of tetrahedral and octahedral sites involves a variable cationic distribution between these non-equivalent crystallographic sites. These cationic arrangements can be described thanks to the inversion degree λ.. Chemical formula of a spinel like AB_2O_4 is written as: $A^{2+}_{1-2\lambda}B^{3+}_{2\lambda}[A^{2+}_{2\lambda}B^{3+}_{2-2\lambda}]O_4{}^{2-}$ (octahedral sites are represented into brackets). The λ = 0 spinel is called « normal » spinel $A[B_2]O_4$ (eg: $NiFe_2O_4$) and for λ = 0.5, spinel is called « inverse » $B[AB]O_4$ (eg: Fe_3O_4). In the studies of Gillot et al. [23,24] and Navrotsky et al. [25], a crystallographic site inversion between Fe^{3+} and Fe^{2+} was observed at high temperature. The authors demonstrated that:

- Fe^{3+} is more stable in octahedral sites.
- Fe^{2+} is stable in both octahedral and tetrahedral sites.

A substitution phenomenon between Fe^{3+} and Al^{3+} can occur as these two ions have the same oxidation degree, and their ionic radii are very similar: 56 pm and 57 pm for Fe^{3+} and Al^{3+} respectively [24].

The substitution reaction can be resumed as:

$$Fe^{3+}[Fe^{2+}Fe^{3+}]O_4^{2-} + Al^{3+} \rightarrow Fe^{3+}[Fe^{2+}Al^{3+}]O_4^{2-} + Fe^{3+} \quad (3a)$$

$$Fe_3O_4 + Al^{3+} \rightarrow Fe_2AlO_4 + Fe^{3+} \quad (3b)$$

However, the composition of the observed phase is $FeAl_2O_4$ and not Fe_2AlO_4 as expected. As the remaining Fe^{3+} in the Fe_2AlO_4 structure are located on tetrahedral site, a site inversion between the two cations Fe^{3+} and Fe^{2+} can explain the composition of the aluminate: Fe^{3+} is then situated in octahedral sites, and Fe^{2+} in tetrahedral sites.

The global aluminate formation mechanism is proposed to be:

$$Fe^{3+}[Fe^{2+}Fe^{3+}]O_4^{2-} + Al^{3+} \rightarrow Fe^{3+}[Fe^{2+}Al^{3+}]O_4^{2-} + Fe^{3+} \quad \lambda = 0.5 \quad (4)$$

$$Fe^{3+}[Fe^{2+}Al^{3+}]O_4^{2-} \rightarrow Fe^{2+}[Fe^{3+}Al^{3+}]O_4^{2-} \quad (5)$$

$$Fe^{2+}[Fe^{3+}Al^{3+}]O_4^{2-} + yAl^{3+} \rightarrow Fe^{2+}[Fe^{3+}_{1-y}Al^{3+}_{1+y}]O_4^{2-} + yFe^{3+} \quad \lambda = 0 (0 < y < 1) \quad (6)$$

Kinetics studies were performed at 960 °C in LiF – CaF_2 – AlF_3 (2.5 wt%) to evaluate the $FeAl_2O_4$ formation rate and Fe_3O_4 pellets were dipped for 2 h, 5 h, 7 h and 14 h at 960 °C. $FeAl_2O_4$ amount is determined by optical microscopy, by calculating the difference between the initial surface area and the transformed one (the zone in which the aluminium has been substituted for iron). The modified surface area was checked to be homogeneous along the entire sample length, allowing to calculate a modified volume. Then, the total quantity of remaining Fe_3O_4 in the material (in mole) was estimated thanks to the molar volume ($44.56\ cm^3.mol^{-1}$).

A zero-order kinetic system is assumed, and is characterized by a linear relationship between remaining quantity and duration:

$$n = n_0 - kt \quad (7)$$

where k is the kinetic constant of the reaction and n_0 the Fe_3O_4 initial quantity of mole.

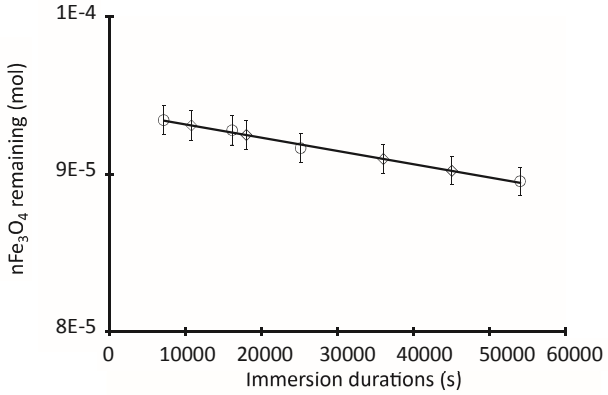

Fig. 4. Variation of the remaining quantity of Fe_3O_4 (moles) versus the immersion durations in LiF – CaF_2 at 960 °C for 2.5 wt% (circle) and 5 wt% of AlF_3 (rhombus).

The remaining quantity of Fe_3O_4 mole (n_{Fe3O4}) is represented *vs* the immersion durations in Fig. 4 for two AlF_3 contents (2.5 and 5 wt%).

Both conditions leaded to the same linear relationship at 960 °C, proving the assumption of zero-order kinetics, independent of AlF_3 concentration:

$$n_{Fe_3O_4(mol)} = 9.4.10^{-5} - 8.4.10^{-11}t_{(s)} \quad (8)$$

The $FeAl_2O_4$ formation kinetic constant value was determined: $k_{FeAl2O4\ formation} = 8.4.10^{-11}\ mol{\cdot}s^{-1}$ at 960 °C.

3.2. *Fe_3O_4 stability in molten cryolite*

Studies performed into LiF – CaF_2 – AlF_3 bath demonstrated that $FeAl_2O_4$ aluminate was spontaneously formed when contacting the salt and the spinel. As suggested by Jentoftsen et al. [16], the aluminate is soluble into molten cryolite. In order to determine the Fe_3O_4 dissolution mechanism, immersion of Fe_3O_4 pellet was performed for 4 h at 960 °C in molten cryolite bath. Micrographic analysis of this pellet is presented in Fig. 5, where $Fe_{1.3}Al_{1.7}O_4$ is detected at the material/salt interface and the initial Fe_3O_4 in the bulk.

The total substitution of Fe^{3+} by Al^{3+} (y = 2) corresponding to $FeAl_2O_4$ is never observed, confirming its solubility in the cryolitic bath.

Kinetic studies were performed in cryolite to estimate the Fe_3O_4 dissolution rate and displayed in Fig. 6. The material dissolution was measured by optical microscopy where a decrease of its dimensions was observed. The same procedure to estimate the remaining quantity of Fe_3O_4 (§3.b) was used in cryolitic bath. Fe_3O_4 pellets were dipped in cryolitic bath for 30 min, 45 min, 2 h, 4 h, 5 h, 7 h and 14 h at 960 °C.

A straight line is obtained, with the linear equation at 960 °C:

$$n_{Fe_3O_4(mol)} = 9.4.10^{-5} - 1.6.10^{-9}t_{(s)} \quad (9)$$

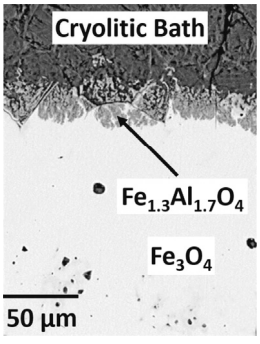

Fig. 5. SEM image of Fe_3O_4 pellet after immersion in Na_3AlF_6 – AlF_3 – CaF_2 – Al_2O_3 bath for 4 h at 960 °C.

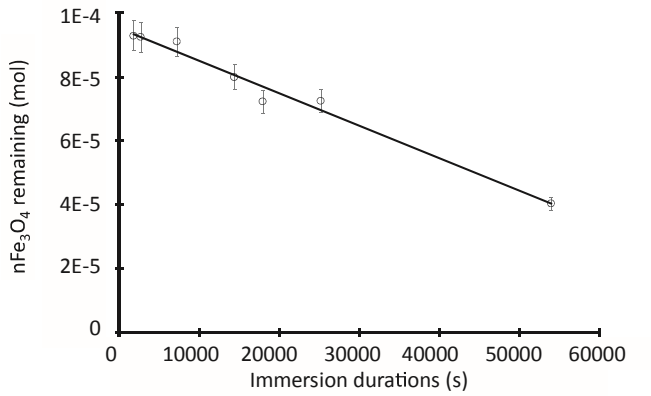

Fig. 6. Variation of the remaining quantity of Fe_3O_4 (moles) versus the immersion durations in Na_3AlF_6 – AlF_3 – CaF_2 – Al_2O_3 at 960 °C.

Fe_3O_4 material dissolution into Na_3AlF_6 – AlF_3 – CaF_2 – Al_2O_3 is also a zero-order kinetics, and the Fe_3O_4 dissolution kinetic constant is $k_{Fe3O4\ dissolution} = 1.6.10^{-9}$ mol·s^{-1} at 960 °C.

By comparing the two kinetic constant values at the same temperature (960 °C), the Fe_3O_4 dissolution one is around twentyfold higher than the $FeAl_2O_4$ formation, explaining why $FeAl_2O_4$ is never detected at Fe_3O_4/salt interface in cryolite. This result indicates that aluminium amount into the obtained aluminate compound increases continuously during immersion (only $Fe_{1.3}Al_{1.7}O_4$ is detected). Then, when aluminium content becomes higher than 1.7, the aluminate compound is rapidly dissolved into molten cryolite, increasing the global material degradation rate.

3.3. Ni impact on $Ni_xFe_{3-x}O_4$ stability

To prevent $FeAl_2O_4$ formation, insertion of nickel in the oxide structure up to $NiFe_2O_4$ is proposed (x = 1). The same immersion conditions were performed on $NiFe_2O_4$ pellet in LiF – CaF_2 – AlF_3 (2.5 wt%) bath at 960 °C and micrographic analysis is presented in Fig. 7.

Navrotsky et al. [26] showed that Ni^{2+} is thermodynamically stable on octahedral crystallographic sites only, so Ni addition prevents the site inversion as only iron from the octahedral sites are substituted. The reaction is then:

$$Fe^{3+}[Ni^{2+}Fe^{3+}]O_4^{2-} + Al^{3+} \rightarrow Fe^{3+}[Ni^{2+}Al^{3+}]O_4^{2-} + Fe^{3+} \quad \lambda = 0 \tag{10a}$$

$$NiFe_2O_4 + Al^{3+} \rightarrow NiFeAlO_4 + Fe^{3+} \tag{10b}$$

EDX analyses show $NiFeAlO_4$ formation at the material/salt interface, whereas the bulk of the material is unchanged ($NiFe_2O_4$). As assumed, no $NiAl_2O_4$ aluminate was formed, proving that the site inversion is blocked. The experiment was repeated with a higher AlF_3 concentration (5 wt%), and the same result was obtained.

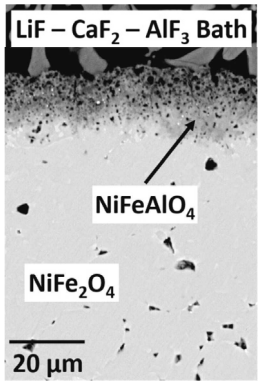

Fig. 7. SEM image of $NiFe_2O_4$ pellet after immersion for 14 h in LiF – CaF_2 – AlF_3 (2.5 wt %) bath at 960 °C.

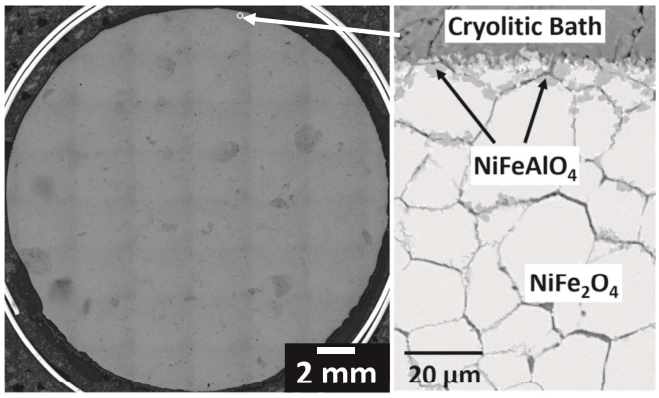

Fig. 8. SEM and optical images of $NiFe_2O_4$ pellet after immersion for 14 h in Na_3AlF_6 – AlF_3 – CaF_2 – Al_2O_3 bath.

The same experiment was performed in Na_3AlF_6 – AlF_3 – CaF_2 – Al_2O_3 bath and micrographic results after grain boundaries revelation are shown in Fig. 8, where no difference is observed between the two solvents. Moreover, no change of the pellet size was observed, showing a good spinel oxide stability in cryolite without polarization.

Despite a good chemical stability in molten cryolite, $NiFe_2O_4$ cannot be used as inert anode due to its very low electrical conductivity (0.8 S·cm^{-1}) [27]. Every Fe^{2+} is replaced by Ni^{2+}, so electrical conduction ensured by electron hopping between Fe^{2+}/Fe^{3+} is impossible. A compromise would be to adjust Ni^{2+} content to keep a sufficient electrical conductivity and to slow down the chemical degradation.

4. Conclusions

Stability of Fe_3O_4 and $NiFe_2O_4$ spinels in molten fluorides at high temperature were examined without polarization. When Fe_3O_4 was dipped into LiF – CaF_2 – AlF_3 bath, a $FeAl_2O_4$ phase is spontaneously formed at the material/salt interface. The proposed mechanism of the aluminate formation is:

1st step: substitution between Fe^{3+} located in octahedral site and Al^{3+} from the bath:

$$Fe^{3+}[Fe^{2+}Fe^{3+}]O_4^{2-} + Al^{3+} \rightarrow Fe^{3+}[Fe^{2+}Al^{3+}]O_4^{2-} + Fe^{3+} \quad \lambda = 0.5$$

2nd step: site inversion between Fe^{3+} located in tetrahedral site and Fe^{2+} in octahedral site:

$$Fe^{3+}[Fe^{2+}Al^{3+}]O_4^{2-} \rightarrow Fe^{2+}[Fe^{3+}Al^{3+}]O_4^{2-}$$

3rd step: substitution between Fe^{3+} located in octahedral site and Al^{3+} from the bath:

$$Fe^{2+}[Fe^{3+}Al^{3+}]O_4^{2-} + Al^{3+} \rightarrow Fe^{2+}[Al^{3+}]_2O_4^{2-} + Fe^{3+} \quad \lambda = 0$$

Kinetic studies were then performed on the aluminate formation rate, and the $FeAl_2O_4$ formation kinetic constant was determined: $8.4.10^{-11}$ mol·s^{-1} and Fe_3O_4 dissolution kinetic constant at 960 °C was $1.6.10^{-9}$ mol·s^{-1}. The ratio between aluminate formation and Fe_3O_4 dissolution is around 20, demonstrating the $FeAl_2O_4$ high solubility.

In order to prevent the Fe^{2+}/Fe^{3+} site inversion leading to soluble $FeAl_2O_4$, Ni^{2+} was added into the spinel structure to form $NiFe_2O_4$ spinel. Its immersion in both molten salts at 960 °C showed the formation of a stable $NiFeAlO_4$ aluminate, inhibiting the material dissolution. However, $NiFe_2O_4$ cannot be used as inert anode because of its too low electrical conductivity. A compromise would be to adjust Ni^{2+} amount, to keep a sufficient electrical conductivity and to slow down the chemical degradation.

Acknowledgements

This work was supported by the French Research National Agency program ANR-13-RMNP-0012.

References

[1] Charles-M. Hall, USPatent 400766, 1889.
[2] R.P. Pawlek, Inert anodes: an update, Light Metals (2002) 449–456.
[3] M. Oudot, L. Cassayre, P. Chamelot, M. Gibilaro, L. Massot, M. Pijolat, S. Bouvet, Layer growth mechanisms on metallic electrodes under anodic polarization in cryolite-alumina melt, Corros. Sci. 79 (2014) 159–168.
[4] S. Helle, M. Pedron, B. Assouli, B. Davis, D. Guay, L. Roué, Structure and high-temperature oxidation behaviour of Cu-Ni-Fe based alloys prepared by high-energy ball milling for application as inert anodes fort aluminium electrolysis, Corros. Sci. 52 (2010) 3348–3355.
[5] I. Gallino, M.E. Kassner, R. Busch, Oxidation and corrosion of highly alloyed Cu–Fe–Ni as inert anode material for aluminium electrowinning in as-cast and homogenized conditions, Corros. Sci. 63 (2012) 293–303.
[6] E. Olsen, J. Thonstad, Nickel ferrite as inert anode in aluminium electrolysis: part II – material performance and long-term testing and preliminary testing, J. Appl. Electrochem. 29 (1999) 301–311.
[7] P. Zarrabian, M. Kalantar, S.S. Ghasemi, Fabrication and characterization of nickel ferrite based inert anodes for aluminium electrolysis, J. Mater. Eng. Perform. 23 (2014) 1656–1664.
[8] R.P. Pawlek, Inert anodes: an update, Light Metals 2014 (2014) 1309–1313.
[9] Z.L. Tian, Y.Q. Lai, J. Li, Z.Y. Li, K.C. Zhou, Y.X. Liu, Effect of Cu-Ni content on the corrosion resistance of (Cu-Ni)/(10NiO-90$NiFe_2O_4$) cermet inert anode for aluminium electrolysis, Acta Metal. Sin. 21 (2008) 72–78.
[10] E. Olsen, Nickel ferrite and tin oxide as anode materials for aluminium electrolysis, PhD, Trondheim University, 1995.
[11] E. Olsen, J. Thonstad, Nickel ferrite as inert anode in aluminium electrolysis: part I – material fabrication and preliminary testing, J. Appl. Electrochem. 29 (1999) 293–299.
[12] E.J.M. Verwey, P.W. Haayman, F.C. Romeijn, Physical properties and cation arrangement of oxides with spinel structures – II. Electronic conductivity, J. Chem. Phys. 15 (1947) 181–187.
[13] D.H. De Young, Solubilities of oxides for inert anodes in cryolithe-based melts, Light Metals 2 (1986) 299–307.
[14] Y. Xiao, M. Pownceby, G. Brooks, Corrosion behavior of nickel ferrite-based ceramics for aluminium electrolysis cell, Light Metals (2007) 909–913.
[15] L. Cassayre, P. Chamelot, L. Arurault, L. Massot, P. Taxil, Oxidation of stoichiometric nickel ferrites used as inert anodes for aluminium electrolysis in molten cryolite mixtures, Mater. Sci. Forum 595–598 (2008) 593–600.
[16] T.E. Jentoftsen, J. Thonstad, E.W. Dewing, G.M. Haarberg, Solubility of FeO and FeAl2O4 in cryolite-alumina melts, J. Electrochem. Soc (1999) 473–484.
[17] L. Baogang, Z. Kechao, L. Zhiyou, Z. Dou, Z. Lei, Microstructure and DC electrical conductivity of spinel nickel ferrite sintered in air and nitrogen atmospheres, Materresbull 45 (2010) 1668–1671.
[18] S. Nightingale, R. Longbottom, B. Monaghan, Corrosion of nickel ferrite refractory by Na3AlF6–AlF3–CaF2–Al2O3 bath, J. Eur. Ceram. Soc. 33 (2013) 2761–2765.
[19] P. Chamelot, B. Lafage, P. Taxil, Studies of niobium electrocrystallization phenomena in molten fluorides, J. Electrochem. Soc. 143 (1996) 1570–1576.
[20] S. Corso, P. Tailhades, I. Pasquet, A. Rousset, V. Laurent, A. Gabriel, C. Condolf, Solid State Sci. 6 (2004) 791–798.
[21] B.A. Wechsler, D.H. Lindsley, C.T. Prewitt, Am. Mineral. 69 (1984) 754.
[22] R. Langley, A. Mouton, F. Stephen Austin, State Univ., Nacogdoches, TX, USA., Private Communication, 2003.
[23] M. Kergoat, Evaluation de la fluoroacidité en milieux de sels fondus, PhD, Université Paul Sabatier, 2014.
[24] B. Gillot, J. Tyranowicz, A. Rousset, Etude de la cinétique d'oxydation de magnétites finement divisées – Influence de la substitution par l'aluminium, Mat. Res. Bull. 10 (1975) 775–782.
[25] B. Gillot, A. Rousset, On the limit of aluminium substitution in Fe3O4 and γ-Fe2O3, Phys. Stat. sol. (a) 118 (1990) K5–K8.
[26] A. Navrotsky, O.J. Kleppa, The thermodynamics of cation distributions in simple spinels, J. Inorg. Nucl. Chem. 29 (1967) 2701–2714.
[27] H. Zhang, V. De Nora, J.A. Sekhar, Materials used in the Hall-Héroult cell for aluminium production, TMS, Warrendale, Pennsylvania, 1994.